

Physical Simulation of Investment Casting of Complex Shape Parts

MEHDI RAHIMIAN, SRDJAN MILENKOVIC, LAURA MAESTRO,
AITOR EGUIDAZU RUIZ DE AZUA, and ILCHAT SABIROV

Development of investment casting process has been a challenge for manufacturers of complex shape parts. Numerous experimental casting trials are typically carried out to determine the optimum casting parameters for fabrication of high-quality products. In this work, it is demonstrated that physical simulation of investment casting can successfully predict microstructure and hardness in as-cast complex shape parts. The physical simulation tool consists of a thermal model and melting/solidification experiments in thermo-mechanical simulator. The thermal model is employed to predict local cooling rate during solidification at each point of a casting. Melting/solidification experiments are carried out under controlled cooling rates estimated by the thermal model. Microstructural and mechanical characterization of the solidified specimens is performed; the obtained results predict the local microstructure and mechanical properties of the casting. This concept is applied to investment casting of complex shape nozzle guide vanes from Mar-M247 Ni-based superalloy. Experimental casting trials are performed and the outcomes of physical simulation tool are validated against experimental results. It is shown that phase composition, secondary dendrite arm spacing, grain size, γ/γ' eutectic size and volume fraction, size and shape of carbide particles, and local microhardness can be predicted at each point of the casting *via* physical simulation.

DOI: 10.1007/s11661-015-2815-6

© The Minerals, Metals & Materials Society and ASM International 2015

I. INTRODUCTION

INVESTMENT casting process, known as a lost wax casting or precision casting, is a well established process for production of near net-shape components. Due to excellent surface finish and dimensional accuracy, this process is especially useful for casting of complex shape containing thin sections.^[1] This manufacturing technique has been widely used for fabrication of various parts (such as disks, stators, nozzle guide vanes (NGV), *etc.*) for aero-engines and gas turbines. As these parts are exploited at high temperatures and aggressive environments, they are typically made from high-density Ni-based superalloys showing high strength, excellent oxidation, and creep resistance at such service conditions.^[2] The search for reduced weight and increased efficiency of aero-engines and gas turbines is driving changes in design of parts to more complex shapes and thinner geometries. However, these innovations are often hindered by the complexity of investment casting

of parts with thin elements. Development of investment casting routes for the complex shape parts is usually carried out *via* a 'trial and error' approach or, in other words, *via* experimental casting trials. The casting parameters are varied until good quality castings are produced. However, this strategy is very expensive and time consuming.^[3] Modeling of investment casting is another approach to determine the optimum casting parameters.^[4] Simulation of casting is reliable when the accurate data of materials are known at processing conditions, and boundary conditions are defined precisely. Casting simulation was applied by Gonzales *et al.*^[5] to visualize mold filling and heat transfer during casting and solidification in order to predict microstructure and location of internal defects. The existing casting simulation tools are able to predict the local thermal profile, local grain structure, and defects (gas porosity, shrinkage pores, *etc.*) in the as-solidified complex shape parts.^[6] However, precise prediction of local phase composition, second phase precipitates, segregations, *etc.*, is out of capabilities of the current casting simulation tools, whereas these microstructural features significantly affect the local mechanical and functional properties in the castings from Ni-based superalloys.

Physical simulation of metallurgical processes is often employed for development of novel manufacturing routes. Physical simulation involves the exact reproduction of the thermal and mechanical processes in the laboratory, as the material has to undergo in the full scale fabrication process. There is a body of research where physical simulation of continuous casting was successfully performed. In the continuous casting, the

MEHDI RAHIMIAN, Research Assistant, SRDJAN MILENKOVIC, Researcher, Head of Solidification Processing and Engineering Group, and ILCHAT SABIROV, Senior Researcher, Head of Physical Simulation Group, are with the IMDEA Materials Institute, Calle Eric Kandel 2, 28906 Getafe, Madrid, Spain. Contact e-mail: ilchat.sabirov@imdea.org LAURA MAESTRO, Simulation Engineer, and AITOR EGUIDAZU RUIZ DE AZUA, Process Engineer, are with the Precicast Bilbao, El Carmen s/n, 48901 Barakaldo, Spain.

Manuscript submitted October 17, 2014.

Article published online February 27, 2015

Table I. Chemical Composition of MAR-M247 Ni-Based Superalloy

Elements	C	Cr	Mo	Ti	Co	W	Ta	Al	Hf	B	Zr	Ni
Content (wt pct)	0.15	8	0.6	1	10	10	3	5.5	1.5	0.02	0.03	bal.

liquid metal is poured into a crystallizer chamber in which its outer shell has to solidify to the extent securing the liquid core inside. When a vertically cast slab or billet has to be bent into horizontal position, the ductility of outer shell must allow this. Gaining physical data for such operation includes melting/solidification experiments on numerous samples followed by hot tensile testing them at various temperatures after solidification, to create hot ductility maps, as it was done for steel by Suzuki et al.^[7] Michalik and Kolmasiak performed physical simulation of continuous casting of St2S steel in order to predict internal stresses and their relaxation during metallurgical process.^[8] Ferguson *et al.* described another technique which was developed specifically to simulate continuous casting followed by semi-solid or direct *in situ* hot rolling.^[9] This metallurgical process is characterized by complex three-dimensional heat flow which is determined by the melt temperature, the temperature of the walls of the caster, the geometry and thickness of the slab, and the velocity of the slab. The modes and directions of solidification directly affect the dendritic and grain structure and impurity segregations in the as-solidified slab. The HDSV40CC-DR simulator can control multiple dimensions of heat flow while performing semi-solid deformation for a physical simulation that closely simulates the real process. Various multi-state forming and multi-stage cooling combinations can be carried out in this way. Temperature, strain, strain rate, force, and cooling rates can all be controlled and measured precisely to yield a quantitatively understood experiment. The investment casting process is also characterized by complex three-dimensional heat flow determined by numerous casting parameters including melt temperature, temperature of ceramic mold, casting shape, thermo-physical properties of ceramic mold and metal, *etc.* Thus, significant variations of local cooling rate during solidification of complex shape part can be expected in its different sections. As it is well known, the thermal profile during solidification and cooling process can significantly affect the local dendritic structure, grain structure, phase composition, thus, resulting in varying local properties over as-solidified parts. Combination of thermal model, predicting local cooling rate at each point of the casting, and melting/solidification experiments in thermo-mechanical simulator under controlled cooling rate, obtained *a priori* by thermal model, should generate a reliable databank for prediction of local microstructure in the as-cast parts.

The main objective of this work is to present a novel tool for physical simulation of investment casting of complex shape parts. In the present work, this tool was applied to the investment casting process of NGV from Mar-M247 Ni-based superalloy.

II. MATERIAL

MAR-M247 Ni-based superalloy was chosen as a material for this investigation. The material was developed in the very early 1970s by Danesi, Lund, and others at the Martin Metals Corporation. It demonstrates high creep strength and good castability along with excellent oxidation resistance.^[10]

The superalloy was supplied by Precicast Bilbao (Bilbao, Spain). Its chemical composition is shown in Table I.

III. PHYSICAL SIMULATION OF INVESTMENT CASTING

The tool for physical simulation of investment casting consists of thermal model, melting solidification experiments in a thermo-mechanical simulator, and microstructural and mechanical characterization of the melted/solidified specimens, as demonstrated schematically in Figure 1. In the present work, the ProCast-based thermal model was applied to predict local cooling rates at defined points of NGV. The outcomes from modeling, namely cooling rates, served as input parameters for the melting/solidification experiments in the thermo-mechanical simulator Gleeble 3800 (Dynamic Systems Inc., Poestenkill, NY, USA). Detailed microstructural and mechanical characterization of the melted/solidified specimens provided a databank on the microstructure and hardness of the material depending on the cooling rate. Finally, experimental casting trials were successfully carried out for validation of the tool (Figure 1).

Physical simulation of investment casting begins with calculation of the local cooling rates during solidification of complex shape part using the ProCast-based thermal model (Figure 1). The obtained data serve as input parameters for melting/solidification experiments in the Gleeble thermo-mechanical simulator that allows to reproduce various local thermal profiles seen by the material during solidification. Thus, obtained specimens are further used for microstructural and/or mechanical characterization. So, the database of microstructure and mechanical properties depending on the local cooling rate is generated to predict the local microstructure and local mechanical properties at each point of casting. Physical simulation process is described in details below.

A. Thermal Model for Investment Casting Process

The basis for reliable physical simulation of investment casting is a very accurate prediction of local cooling rate at each point of the cast. Development of the thermal model requires the optimal selection of the thermo-physical parameters along with the proper

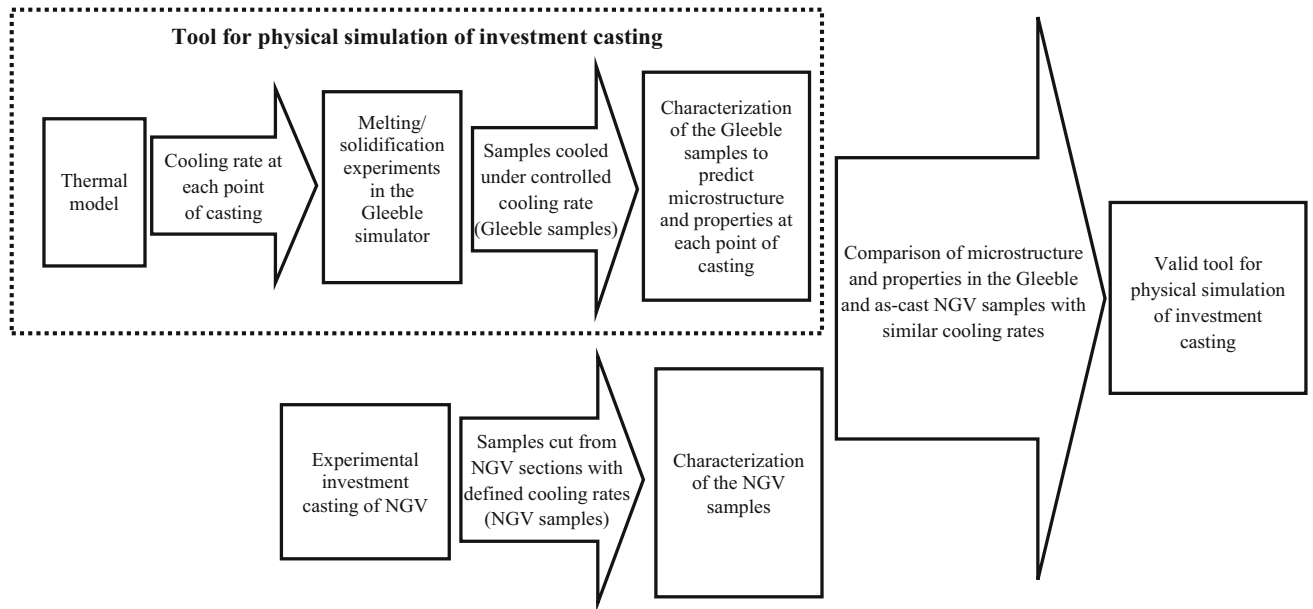


Fig. 1—Schematic presentation of the tool for physical simulation of investment casting and its validation performed in the present work.

establishment of boundary conditions. Mold filling during investment casting was modeled using the three-dimensional finite element solver ProCast (ESI, Lausanne, Switzerland) by solving the conservation of mass, momentum, and heat flow equations.^[1] Conservation of mass is enforced through the continuity equation

$$\frac{\delta \rho}{\delta t} + \frac{\delta(\rho u_i)}{\delta x_i} = 0, \quad [1]$$

where u_i is the corresponding component of the velocity and ρ stands for the density. The momentum equation as used in ProCast is given by

$$\rho \frac{\delta u_i}{\delta t} + \rho u_j \frac{\delta u_i}{\delta x_j} + \frac{\delta}{\delta x_j} \left(p \zeta_{ij} (\mu + \mu_T) \frac{\delta u_i}{\delta u_j} \right) = \rho g_i - \frac{\mu}{Kp} u_i, \quad [2]$$

where ζ_{ij} is the Kronecker delta, p the pressure, g_i the gravitational acceleration, μ the viscosity, μ_T the eddy viscosity, and Kp the permeability. These equations are solved under the assumption that the spatial derivatives of viscosity are small and that the fluid is nearly incompressible.

During investment casting, heat flows by conduction through the metal, ceramic mold, and insulation wrap and is removed from the surface by natural convection and radiation. The heat flow is transient, *i.e.*, the temperatures in the casting, mold, and insulation wrap change with time. The governing partial differential equation of heat flow by conduction is expressed as

$$\rho \frac{\delta H}{\delta T} \frac{\delta T}{\delta t} - \nabla [K \nabla T] - S(r) = 0, \quad [3]$$

where $\nabla = \frac{\partial}{\partial x} + \frac{\partial}{\partial y} + \frac{\partial}{\partial z}$, T stands for the temperature, t for the time, K for the thermal conductivity, $S(r)$ is a spatially varying heat source, and H the enthalpy of

solidification, which encompasses both the specific heat term (c_p) and the evolution of latent heat (L) during solidification according to

$$H(T) = \int_0^T c_p dr + L(1 - f_s(T)), \quad [4]$$

where f_s is the fraction of solid.

Initial and boundary conditions for the resolution of previous equations are applied on temperature, velocity, pressure, fixed turbulent kinetic energy, fixed turbulent dissipation rate, and specific, convective and radiation heat flux. To solve the complex view factor radiation capability, ProCast uses a net flux model. Rather than tracking the reflected radiant energy from surface to surface, an overall energy balance for each participating surface is considered.

An iterative algorithm is used to solve Eq. [2] by finding a coherent solution between enthalpy and temperature results. Further details about the resolution of the solidification phenomena based on enthalpy and temperature can be found in Reference 12.

Several software packages were used to generate the thermal model. The NGV design was created using Solid Works software (Dassault Systems SolidWorks Co., Massachusetts, USA), while the feeding system was created with Unigraphics software (UGS Inc., Texas, USA). Both packages are linked to the casting simulation software ProCast calculating the thermal history of the model. Surface and volume meshes were generated by Visual-Mesh (ESI, Luasanne, Switzerland), considering a maximum distance between nodes of 2 mm inside the NGV. The investment casting ceramic mold was composed of layers which were created by ProCast 2D mesh shelling multi-thickness. The mold maintains its average thickness of 13 mm in the computer model. The insulation wrap having a thickness of 13 mm was

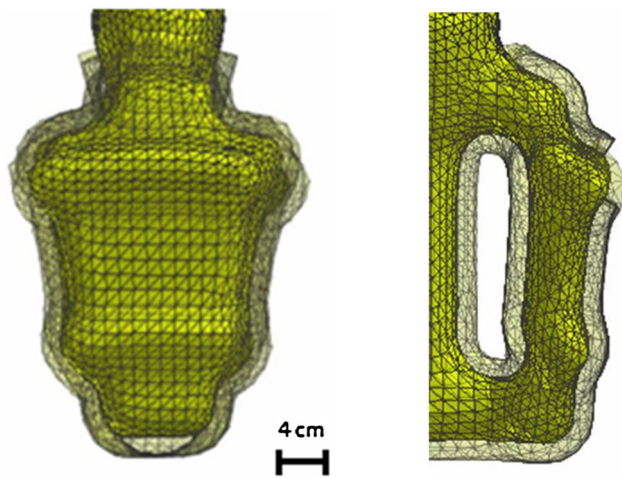


Fig. 2—View of surface and volume meshes (green color corresponds to ceramic mold, gray color corresponds to insulation wrap) (Color figure online).

created and meshed by ProCast 3D mesh layer shell. In order to simplify the geometry of the model and to improve the computational efficiency, only half of the mold was considered due to its symmetry (Figure 2). The detailed description of the thermal model and thermo-physical parameters applied in modeling of investment casting of NGV from Mar-M247 Ni-based superalloys can be found in the very recent manuscript by Torroba *et al.*,^[13] where the model was validated against experimental temperature measurements during casting trials. Its description can also be found in another recent work by Anglada *et al.*^[14]

The thermal calculations were carried out, and the thermal profiles during solidification and cooling were determined for different areas of the casting. In Figure 3(a), typical temperature–time plots predicted by the thermal model for one area with a low cooling rate and for another area with higher cooling rate are presented. Locations of these areas are marked on the as-cast NGV (Figure 3(b)). It is clearly seen that evolution of temperature in the solidification temperature range shows a linear character with time, and the cooling rate can be easily determined for both cases: ~ 0.25 and 1 K/s (~ 0.25 and 1 °C/s) (Figure 3).

B. Melting/Solidification Experiments in Thermo-mechanical Simulator

Cylindrical specimens with the diameter of 10 and 121.5 mm in length were machined from larger ingots of Mar-M247 Ni-based superalloys. The specimens were threaded at both ends. A thin wire R-type thermocouple was welded on the midsection of each specimen to control the temperature during melting/solidification experiments. The liquid melt zone was contained in a ceramic tube with a slot of 3.2 mm, which was put onto each specimen with the thermocouple in the slot (Figure 4). Cement was used to fix the thermocouple to the ceramic tube during experiment (Figure 4(b)).

The melting/solidification experiments were carried out in argon atmosphere using Gleeble 3800 thermo-

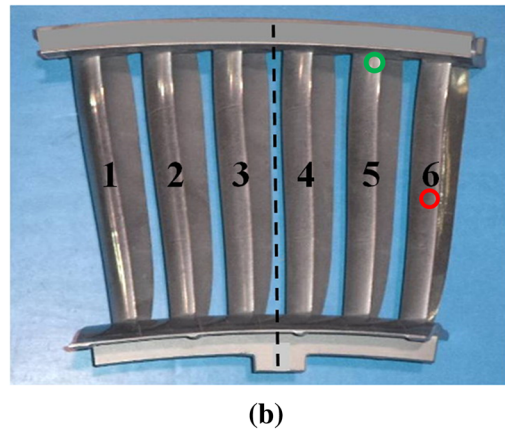
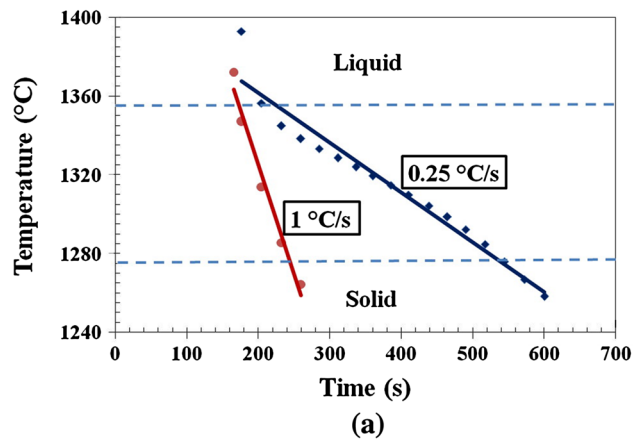


Fig. 3—(a) Theoretical temperature–time plots predicted by thermal model for (b) areas marked by green (cooling rate of 0.25 K/s (0.25 °C/s)) and red (cooling rate of 1 K/s (1 °C/s)) circles on the as-cast NGV (Color figure online).

mechanical simulator. The samples were heated at a rate of 40 K/s to 1513 K (40 °C/s to 1240 °C), then temperature was increased to 1593 K (1320 °C) with the heating rate of 2 K/s (2 °C/s). When the temperature reached 1593 K (1320 °C), it was manually increased slowly up to ~ 1628 K (~ 1355 °C) for full melting. The specimens were held at ~ 1628 K (~ 1355 °C) for 10 seconds and then cooled down by 400 K (400 °C) at two different cooling rates of 0.25 and 1 K/s (0.25 and 1 °C/s), which were calculated by thermal model for some defined sections of NGV (see Section III–A). Afterward, the specimens were cooled in the argon atmosphere to room temperature. The specimens were compressed in a stroke controlled manner during cooling in order to compensate thermal contraction and to suppress formation of shrinkage porosity. Three specimens were tested for each condition and the results were reproducible. The experimental temperature–time plots are illustrated in Figure 5. It is seen that cooling rate was well controlled in both cases. Samples for further microstructural characterization were cut from midsection of the melted and solidified specimens. Hereafter, these samples will be referred to as Gleeble samples.

The microstructure of the midsection area under welded thermocouple of the Gleeble samples was carefully analyzed. The standard metallographic tech-

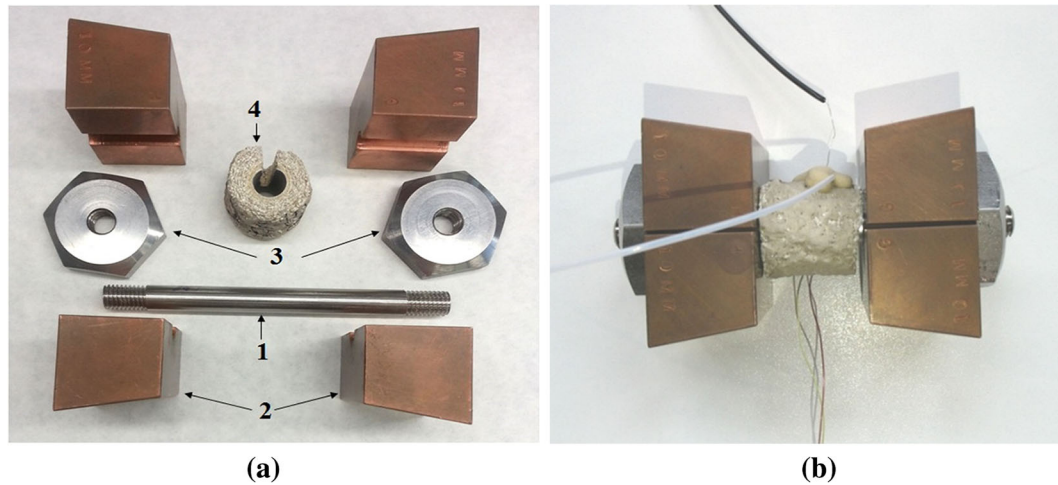


Fig. 4—(a) Parts of the experimental set-up for melting/solidification experiments in the Gleeble 3800 thermo-mechanical simulator: 1-sample, 2-copper grips, 3-nuts, 4-ceramic tube, (b) the set-up ready for maintenance in the Gleeble chamber for melting/solidification experiment.

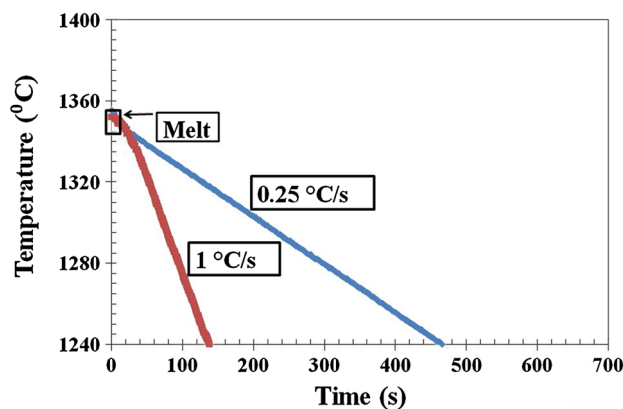


Fig. 5—Typical temperature–time plots from melting/solidification experiments in the thermo-mechanical simulator.

niques were used for preparation of specimens with mirror-like surface. The surface was etched using chemical solution containing 25g FeCl_3 , 60 mL HCl, and 25 mL H_2O to reveal grain boundaries and dendritic microstructure. The optical microscope OLYMPUS BX51 (Olympus Co., Tokyo, Japan) was employed to study grain and dendritic structure. The ANALYSIS software (Olympus Co., Tokyo, Japan) was used for quantitative analysis of microstructure. The measurement of secondary dendrite arm spacing (SDAS) was done by counting the number of secondary arms over a measured length on at least five well-defined trunks. Analysis of carbide particles was done in scanning electron microscope (SEM) EVO MA 15 (Zeiss Co., Jena, Germany) operating at 18 kV. Equivalent circle diameter (ECD) of grains and carbide particles was considered due to their complex shape. Microhardness of the Gleeble samples was measured using SHIMADZU HMV-2 (Shimadzu Corp., Kyoto, Japan) microhardness tester with Vickers diamond indenter. In this test, the 300 g load was applied for 15 seconds. At least ten measurements were done on each selected area. The average microhardness values and their standard deviation were calculated.

C. Experimental Investment Casting of NGV for Validation of Physical Simulation Tool

Experimental casting trials of real NGV were carried out for validation of physical simulation tool (Figure 1). The ceramic molds for the experimental casting trials were prepared using the standard manufacturing route. The wax pattern of NGV was prepared *via* injection molding and then assembled with a wax feeding system. The obtained wax cluster was immersed into a ceramic slurry and allowed to dry, and this step was repeated until the desired thickness of ceramic mold was reached. The obtained assembly was dewaxed in autoclave for 15 minutes at elevated temperature and high pressure. To burn the wax remains, the ceramic cluster was fired at 1173 K (900 °C) for 1 hour. The interior of ceramic cluster was cleaned by alcohol. The ceramic cluster was wrapped by an insulation layer (made from Kaolin wool) having a thickness of 13 mm and pre-heated to 1473 K (1200 °C). The pre-heated assembly was placed in the vacuum casting furnace where the ceramic mold was filled by the molten metal poured at 1822 K (1549 °C) with a melt pouring velocity of 1700 mm/s. The assembly was then removed from the furnace and allowed to cool.

The as-cast NGV is illustrated in Figure 3(b). The vanes 2 and 5 are solid and other vanes are hollow. Since the as-cast NGV has a symmetrical geometry and the gating system was located in its midsection, it can be assumed that microstructure and properties of the left half of NGV (vanes 1, 2, 3, and left half of platform) are similar to that of the right half of NGV (vanes 6, 5, 4, and right half of platform). Therefore, microstructural characterization of the defined areas in the right part of NGV was performed. Each vane was cut into smaller parts to prepare samples for further microstructural and mechanical characterization. Hereafter, these samples will be referred to as NGV samples. Microstructural analysis of NGV samples was performed on defined spots of areas shown in Figure 6. Information on the analyzed areas for each vane is provided in Table II. According to the outcomes of the thermal model, the

defined spots in these areas have cooling rates during solidification of ~ 0.25 or ~ 1 K/s (~ 0.25 or ~ 1 °C/s) (see Section III-A). Microhardness of these areas was also measured. Preparation of samples and experimental procedures were similar to those described above in Section III-B.

IV. RESULTS AND DISCUSSION

This section describes the microstructure of the Gleeble samples compared with the microstructure of the NGV samples. SDAS, grain structure, phase composition, and morphology of carbides were analyzed, since these are the main microstructural features determining properties of Ni-based superalloys.

A. Secondary Dendrite Arm Spacing

As it is well known, SDAS has a strong effect on mechanical strength of the Ni-based superalloys.^[15] Figure 7 shows dendritic microstructure of Mar-M247 Ni-based superalloy in the Gleeble samples (left images) and in the NGV samples (right images). It is seen that morphology of dendritic structure in the Gleeble samples (Figures 7(a) and (c)) is very similar to that of the NGV samples (Figures 7(b) and (d)) at both cooling rates. The results of SDAS measurements are listed in Table III. The SDAS in the Gleeble samples at cooling rate of ~ 0.25 K/s (~ 0.25 °C/s) (70 ± 12 μm) nearly coincides with SDAS in the NGV samples (66 ± 13 μm). A very good accordance of SDAS in the Gleeble samples and in the as-cast NGV samples is

also observed for cooling rate of 1 K/s (1 °C/s), 35 ± 8 and 39 ± 9 μm , respectively (Table III).

The SDAS values decrease with increasing cooling rate (Table III) that is in a good agreement with the results reported earlier by Zhang *et al.*^[16] and many other research groups. According to Kurz and Fisher,^[17] the SDAS is determined by the total time that a given secondary branch spends in contact with the liquid during solidification process (in other words, by local solidification time) because the diffusion coefficient of the solute is significantly larger in the liquid than in the solid. The local solidification time decreases with increasing cooling rate resulting in finer SDAS.

B. Grain Structure

Figure 8 demonstrates grain structure of the Gleeble samples (Figures 8(a) and (c)) and NGV samples (Figures 8(b) and (d)) at cooling rates of 0.25 K/s (0.25 °C/s) (Figures 8(a) and (b)) and 1 K/s (1 °C/s)

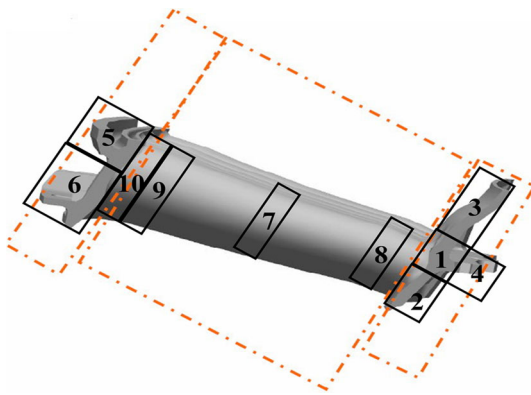


Fig. 6—Schematic view of the NGV with marked areas for microstructural studies.

Table II. Investigated Parts and Areas of the As-cast Investment Casting NGVs

		As-cast NGV								
Vane	4	5				6				
Area	7	5	7	8	9	2	3	4	5	7

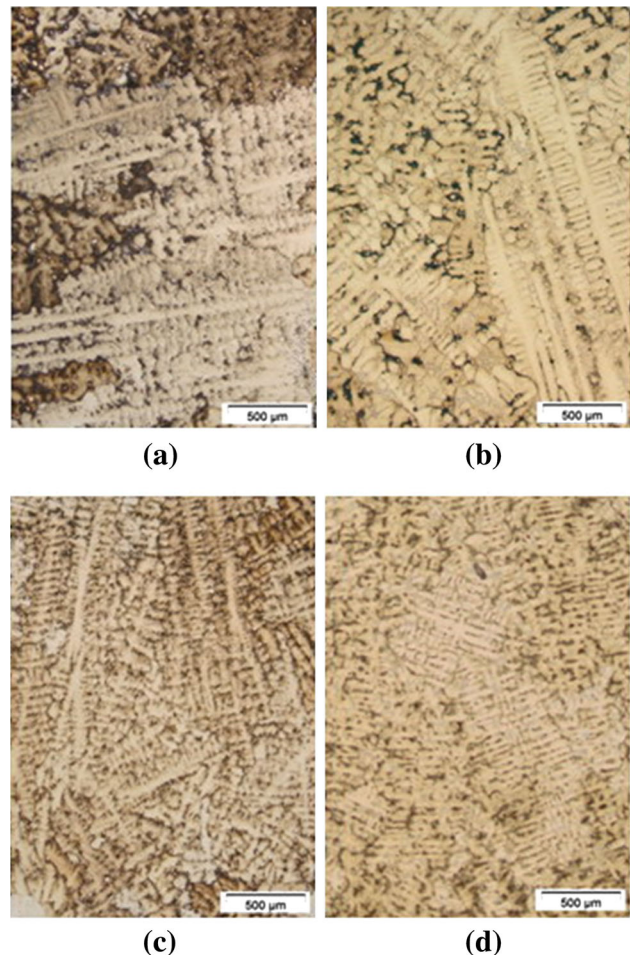


Fig. 7—Dendritic microstructure of (a, c) the Gleeble samples and (b, d) as-cast NGV samples cooled at (a) Gleeble sample, 0.25 K/s (0.25 °C/s), (b) NGV sample (transversal section of the solid vane 5 marked by green circle on Fig. 3(b), 0.25 K/s (0.25 °C/s) and (c) Gleeble sample, 1 K/s (1 °C/s), (d) NGV sample (transversal section of the hollow vane marked by red circle on Fig. 3(b), 1 K/s (1 °C/s).

Table III. Results of Microstructural Characterization and Microhardness Measurements of the Gleeble and NGV Samples (Average Value \pm Standard Deviation)

Processing	Gleeble Samples		NGV Samples	
Cooling rate ($^{\circ}\text{C}/\text{s}$)	0.25	1	0.25	1
SDAS (μm)	70 ± 12	35 ± 8	66 ± 13	39 ± 9
Grain structure				
Grain size (μm)	1279 ± 347	1050 ± 284	1264 ± 693	1018 ± 437
Aspect ratio	2.1	2.36	2.19	2.44
Phase composition				
Carbide				
Size (μm)	8 ± 2	4 ± 2	7 ± 3	4 ± 2
Volume fraction (pct)	1.1	1.8	1.2	1.7
Inter-particle spacing λ (μm)	23 ± 4	9 ± 1	18 ± 2	9 ± 1
γ/γ' eutectic				
Volume fraction (pct)	10.4	3.4	10.2	3.2
Size (μm)	44 ± 9	24 ± 5	41 ± 8	23 ± 6
Microhardness (HV)	382 ± 20	408 ± 15	381 ± 16	415 ± 7

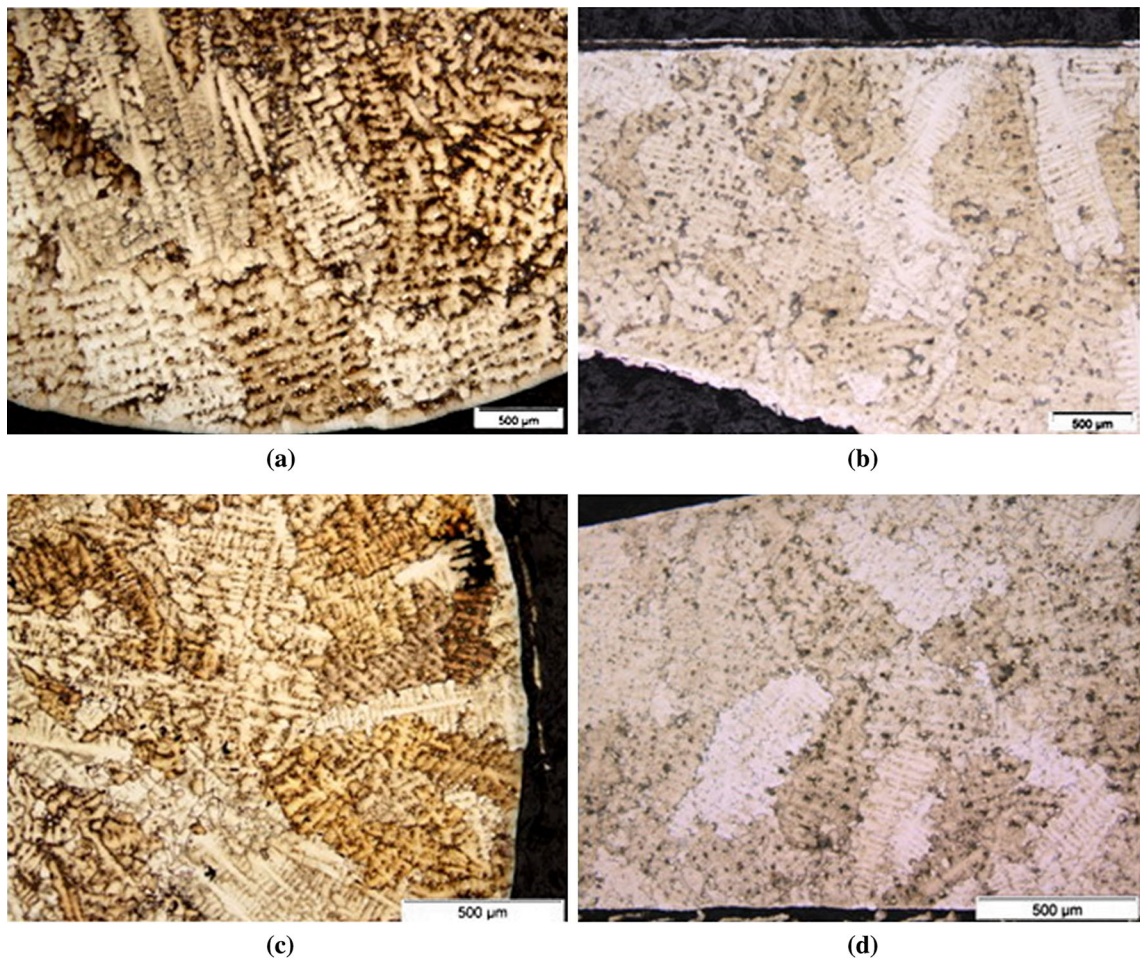


Fig. 8—Grain structure of (a, c) the Gleeble samples and (b, d) as-cast NGV samples cooled at (a) Gleeble sample, 0.25 K/s ($0.25^{\circ}\text{C}/\text{s}$), (b) NGV sample (transversal section of the solid vane 5 marked by green circle on Fig. 3b), $0.25^{\circ}\text{C}/\text{s}$ and (c) Gleeble sample, 1 K/s ($1^{\circ}\text{C}/\text{s}$), (d) NGV sample (transversal section of the hollow vane 6 marked by red circle on Fig. 3b), 1 K/s ($1^{\circ}\text{C}/\text{s}$).

(Figures 8(c) and (d)). It is seen that physical simulation can reproduce well the grain structure of the as-cast NGV at both cooling rates. The average grain sizes in the specimens after physical simulation and in the NGV

are in a good accordance. The average grain size tends to decrease with increasing cooling rate, though the values of standard deviation are high, due to large grain size and small number of grains available for quantita-

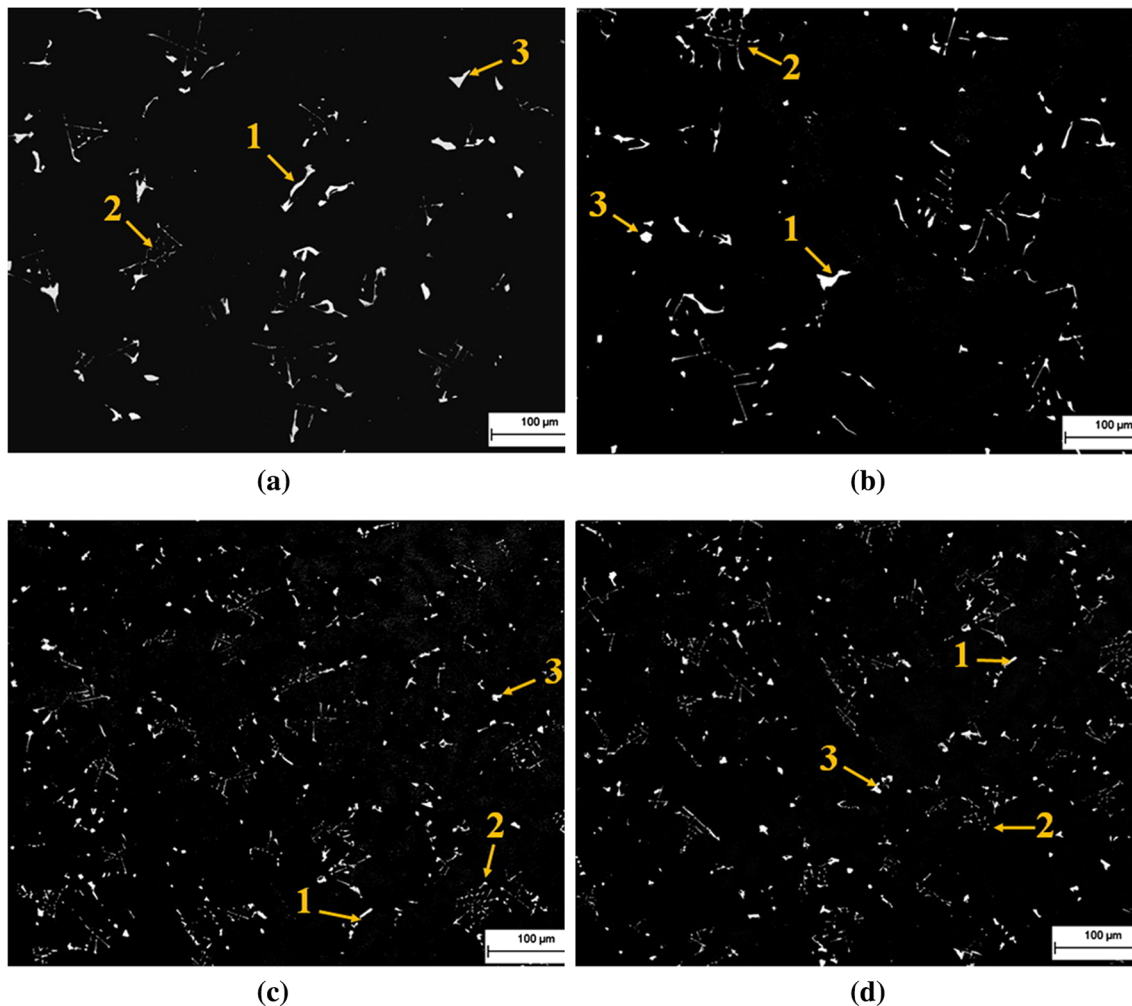


Fig. 9—The carbide characteristics of (a, c) the Gleeble samples and (b, d) as-cast NGV samples cooled at (a) Gleeble sample 0.25 K/s (0.25 °C/s), (b) NGV sample (transversal section of solid vane marked by green circle on Fig. 3b), 0.25 K/s (0.25 °C/s) and (c), Gleeble sample, 1 K/s (1 °C/s), (d) NGV sample (transversal section of hollow vane marked by red arrow on Fig. 3b), 1 K/s (1 °C/s). 1-carbides of irregular shape, 2-script-like carbides, 3-blocky carbides.

tive analysis. Comparing the microstructures, it can be also observed that the morphology of the grains is identical too. This observation is confirmed by comparing the average aspect ratios of the grains (Table III). The values of average aspect ratio of 2.10 and 2.36 obtained in the Gleeble samples for the cooling rates of 0.25 and 1 K/s (0.25 and 1 °C/s) match perfectly with the values of 2.19 and 2.44 in the as-cast NGV samples. However, the average aspect ratio demonstrates the opposite tendency of the grain size, *i.e.*, it slightly increased with the cooling rate.

C. Phase Composition

1. Carbide particles

As it is well known, the morphology, size, and volume fraction of carbide particles can strongly affect mechanical strength and creep resistance of Ni-based superalloys.^[18] Figure 9 depicts the morphology of carbides in the Gleeble samples (Figures 9(a) and (c)) and in the as-cast NGV samples (Figures 9(b) and (d))

cooled at 0.25 K/s (0.25 °C/s) (Figures 9(a) and (b)) and 1 K/s (1 °C/s) (Figures 9(c) and (d)).

It is clearly seen that physical simulation reproduces well morphology of carbide particles at both cooling rates. Various types of carbides (script-like, blocky, and carbides of irregular shape) are observed in the microstructure of all studied specimens. Carbides of irregular shape prevail in the specimens cooled at 0.25 K/s (0.25 °C/s), while script-like carbides dominate in the microstructure of specimens cooled with 1 K/s (1 °C/s). At higher cooling rates, carbides tend to transform into strips, in order to increase the free surface area and thus access large amounts of carbide-forming elements. Further growth and coalescence of these fine strips leads to formation of script-like carbides as observed in the Gleeble and NGV samples cooled at 1 K/s (1 °C/s) (Figures 9(c) and (d)). At low cooling rates, the carbides tend to have equilibrium morphology (in shape of octahedron) in order to minimize carbide-liquid interface energy.^[19] The cooling rate of 0.25 K/s (0.25 °C/s) is still too high for formation of carbides

with equilibrium morphology, so carbides of irregular shapes are mainly formed at this cooling rate.

The increase in cooling rate results in reduction of average carbide size and inter-particle spacing in the as-cast NGV, and this is also well captured in physical simulation (Table III). Volume fraction of carbide particles in the as-cast NGV samples tends to increase from 1.2 to 1.7 pct with increasing cooling rate that is also reproduced by physical simulation, where it increases from 1.1 to 1.8 pct (Table III). It can be rationalized based on reduction of time for diffusion of alloying elements (in other words, carbide growth time) with increasing cooling rate. Smaller SDAS at higher cooling rates results in reduction of carbide inter-particle spacing, since according to He *et al.*,^[20] interdendritic areas are preferred location for segregation of carbide-forming elements and carbide formation in the Ni-based superalloys (Figure 10). Formation of larger number of carbide nuclei together with the smaller interdendritic area could be the reason for increasing carbide volume fraction with increasing cooling rate.

2. The γ/γ' eutectic

In the Ni-based superalloys, γ/γ' eutectic is a non-equilibrium solidification microconstituent caused by segregation of eutectic-forming elements such as Ti and Al in interdendritic areas during solidification process.^[21] Formation of γ/γ' eutectic pools is controlled by chemical composition of the alloy and cooling rate during alloy solidification. Figure 11 illustrates their morphology observed in the Gleeble specimens (Figures 11(a) and (c)) and in the as-cast NGV samples (Figures 11(b) and (d)) cooled at 0.25 K/s (0.25 °C/s) (Figures 11(a) and (b)) and 1 K/s (1 °C/s) (Figures 11(c) and (d)).

The results of their quantitative analysis are listed in Table III. It is seen that physical simulation (Gleeble samples) can very well predict morphology, size, and volume fraction of γ/γ' eutectic pools in the as-cast NGV

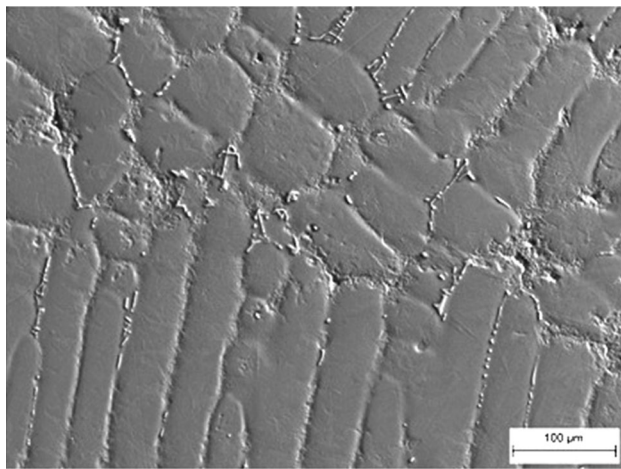


Fig. 10—Carbides in interdendritic area of the Gleeble specimen after solidification with cooling rate of 1 K/s (1 °C/s).

at both cooling rates. Their average size decreases from 41 ± 8 to 23 ± 6 μm with increasing cooling rate in the as-cast NGV, that matches well with the outcomes of physical simulation (Gleeble samples), where it drops from 44 ± 9 to 24 ± 5 μm (Table III). Similar trend is shown by volume fraction of γ/γ' eutectic. Gleeble samples predict its reduction from 10.4 to 3.4 pct with increasing cooling rate that is in a very good accordance with the results for the as-cast NGV, 10.2 and 3.2 pct, respectively (Table III). As demonstrated by Liu *et al.*,^[22] higher cooling rates result in dendrite refinement leading to lower amount of segregations and smaller eutectic pools. It should be noted that no γ/γ' eutectic was observed in the Mar-M247 Ni-based superalloy after physical simulation with cooling rate of 1 K/s (1 °C/s) in our previous work.^[23] This discrepancy in results can be related to possible variations in chemical composition (especially in content of the eutectic-forming elements) of the studied material.

D. Microhardness

The results of microhardness measurements on all studied specimens are listed in Table III. A very good agreement between microhardness data measured on the as-cast NGV and on specimens after physical simulation can be noted. It is seen that the average microhardness values increase with increasing cooling rate from 381 to 415 HV and from 382 to 408 HV in the as-cast NGV and Gleeble samples, respectively. This result can be expected, since microhardness is governed by microstructural features which were very well reproduced in physical simulation (see Sections IV–A to IV–C). Reduction of SDAS with increasing cooling rate (see Section IV–A) improves strength, as was shown in Reference 24. Finer carbides, higher carbide volume fraction, and lower inter-particle spacing in the specimens cooled at higher cooling rate also result in contribution to higher particle strengthening. It should be noted that grain size effect on strength of the material cannot be analyzed in this case, since grains (having size >1 mm, Table III) are by an order of magnitude larger than the radius of plastic zone in microhardness testing (~ 100 μm).

V. ADVANTAGES OF APPLICATION OF PHYSICAL SIMULATION IN DEVELOPMENT OF NEW INVESTMENT CASTING PROCESS

The present work clearly demonstrates that physical simulation of investment casting can precisely predict the local microstructure and properties in the complex shape parts produced *via* investment casting. Therefore, physical simulation can be of great help in development of new investment casting process (investment casting process using new material or investment casting process of new complex shape parts) greatly reducing the amount of required experimental casting trials. Following advantages of application of physical simulation can be noted:

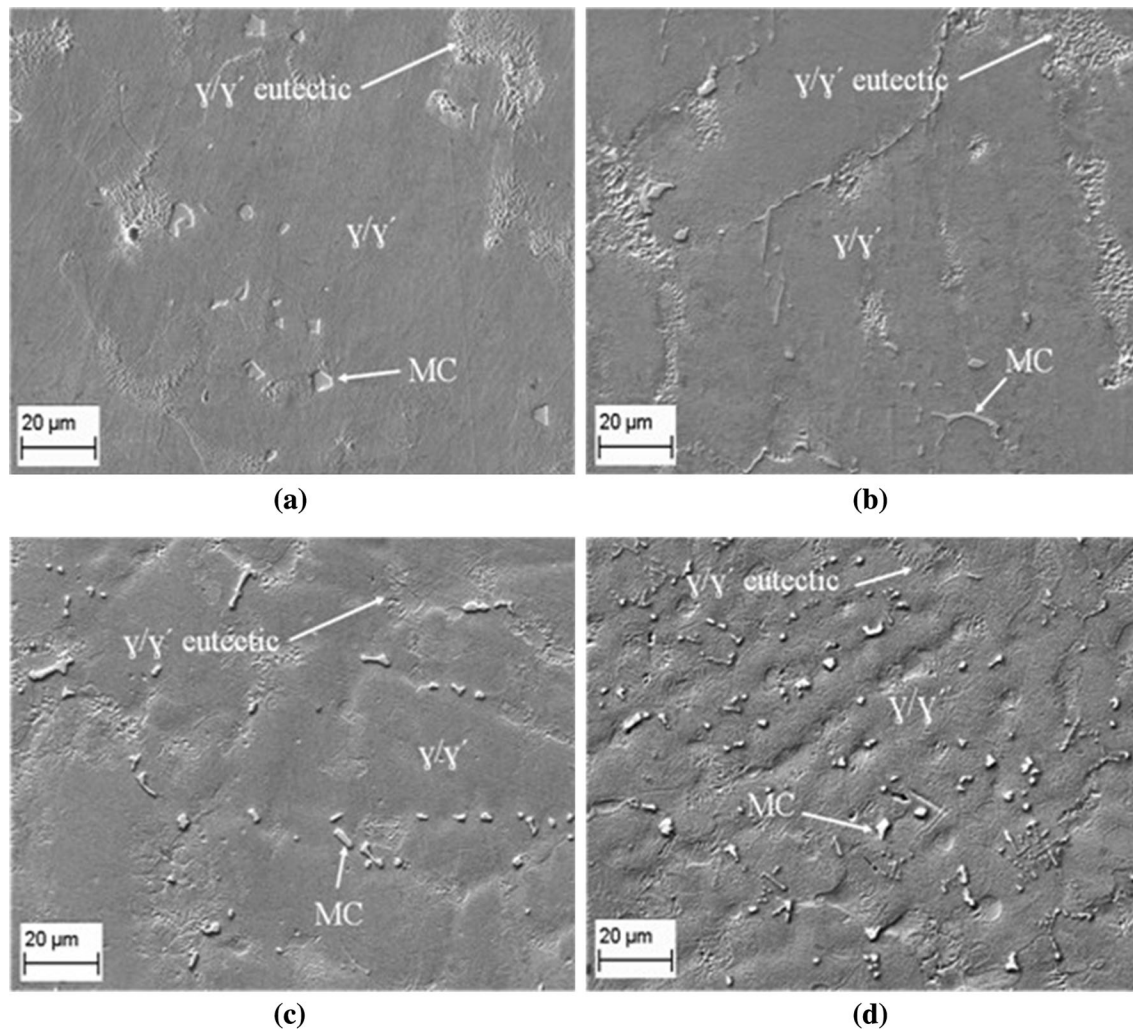


Fig. 11—Microstructure of the (a, c) the Gleeble samples and (b, d) as-cast NGV samples cooled at (a) Gleeble sample, 0.25 K/s (0.25 °C/s) (b) NGV sample (transversal section of solid vane marked by green circle on Fig. 3b), 0.25 K/s (0.25 °C/s) and (c) Gleeble sample, 1 K/s (1 °C/s), (d) NGV sample (transversal section of hollow vane marked by red arrow on Fig. 3b), 1 K/s (1 °C/s).

- (1) *Reduction of material amount required for development of new investment casting process* Significant amount of material typically goes in waste in numerous experimental casting trials required for development of new manufacturing process. The related costs can be very high if expensive materials, as Ni-based superalloys, are used in the investment casting process. Very small specimens used in physical simulation greatly reduce the amount of material required for development of the casting process, thus, reducing its cost.
- (2) *Higher efficiency of experimental work in development of new investment casting process* In the ‘trial-and-error’ approach, as-cast complex shape parts are typically sectioned into small specimens, and careful microstructural analysis is performed in all sections in order to analyze the local microstructure. Such microstructural analysis is especially im-

portant in the case of multiphase materials, where significant variations of local solidification conditions can result in significant variations of local phase composition and, thus, local properties of the complex shape part. Application of physical simulation can significantly increase the efficiency of experimental work: The range of local solidification conditions (*i.e.*, cooling rates) in casting process can be determined by thermal model and further reproduced in the thermo-mechanical simulator. Detailed microstructural analysis of the specimens after physical simulation yields a databank of microstructures present in the as-cast complex shape part. This databank can also be extended to include information on mechanical and/or functional properties of these microstructures, which can be studied using specimens after physical simulation.

- (3) *Direct impact on quality of final product* The as-cast complex shape parts are often subjected to additional homogenization thermal treatments. The obtained databank can be utilized for choosing the optimum parameters of thermal treatments which can improve the quality of final product. For example, the γ/γ' eutectic (which is often formed in Ni-based superalloys solidified at low cooling rates) reduces strength of the material,^[25] and homogenization heat treatment is applied for dissolution of this microconstituent. The areas containing such phases can be missed in microstructural analysis of the sectioned complex shape part, whereas it will be definitely revealed in microstructural analysis of the specimens after physical simulation. The correct choice of thermal treatment parameters for complete dissolution of non-desirable microstructural elements will allow tailoring local microstructures and properties in the as-cast complex shape parts in order to avoid any 'weakest link' in the structure.

VI. CONCLUSIONS

1. Combination of thermal modeling with melting/solidification under controlled cooling rate in thermo-mechanical simulator yields physical simulation of investment casting of complex shape parts. In physical simulation, the local cooling rate during solidification at each point of cast is predicted via thermal modeling. Melting/solidification experiments are carried out under controlled cooling rates determined by the model. Further microstructural and mechanical characterization of the specimens after melting/solidification experiments provides the information on the local microstructure and mechanical properties at each point of the as-cast complex shape part.
2. Physical simulation of investment casting of NGV from MAR-M247 Ni-based superalloy was performed for selected areas of NGV. It is demonstrated that physical simulation predicts well the local SDAS, grain structure, phase composition, morphology of carbide particles, and microhardness.
3. Physical simulation of investment casting has numerous advantages over standard trial-and-error approach for development of new investment casting process. It leads to higher efficiency of experimental work and to reduction of material's amount required for development of the new investment casting process, as well as it improves quality of the final product.

ACKNOWLEDGMENTS

This investigation was carried out in frame of the VANCAS project (EU, FP7, ERA-NET MATERA+). SM and IS acknowledge gratefully the Spanish Ministry of Economy and Competitiveness for financial support through the Ramon y Cajal fellowships.

REFERENCES

1. S. Pattnaik, D.B. Karunakar, and P.K. Jha: *J. Mater. Process. Technol.*, 2012, vol. 212, pp. 2332–48.
2. R.C. Reed: *The Superalloys: Fundamentals and Applications*, Cambridge University Press, Cambridge, 2006.
3. S.T. Mandziej: *Mater. Technol.*, 2010, vol. 44, pp. 105–19.
4. R.W. Hamilton, D. See, S. Butler, and P.D. Lee: *Mater. Sci. Eng. A*, 2003, vol. 343, pp. 290–300.
5. M. Gonzalez, M. Goldschmit, A. Assanelli, E. Dvorkin, and E. Berdaguer: *Metall. Mater. Trans. B*, 2003, vol. 34B, pp. 455–73.
6. J. Guo and M. Samonds: *Modeling of Casting and Solidification Processes*, ASM International, Metals Park, 2010, vol. 22B, pp. 168–95.
7. H.G. Suzuki, S. Nishimura, and S. Yamaguchi: *Proc. Physical Simulation of Welding, Hot Forming and Continuous Casting*, CANMET, Canada, 1988.
8. J. Michalik and C. Kolmasiak: *Metallurgija*, 2009, vol. 48, pp. 71–74.
9. D. Ferguson, W. Chen, T. Bonesteel, and J. Vosburgh: *Mater. Sci. Eng. A*, 2009, vol. 499, pp. 329–32.
10. H.Y. Bor, C.N. Wei, R.R. Jeng, and P.Y. Ko: *Mater. Chem. Phys.*, 2008, vol. 109, pp. 334–41.
11. *ProCast User Manual & Technical Reference*, ESI Software, France, 2007.
12. M. Rappaz, M. Bellet, and M.O. Deville: *Numerical Modelling in Materials Science and Engineering*, Springer-Verlag, Berlin, 2002.
13. A.J. Torroba, O. Koeser, L. Calba, L. Maestro, E. Carreno-Morelli, M. Rahimian, S. Milenkovic, I. Sabirov, and J.L. Lorca: *Integr. Mater. Manuf. Innov.*, 2014, vol. 3, p. 25.
14. E. Anglada, A. Meléndez, L. Maestro, and I. Domiguez: *Proc. Eng.*, 2013, vol. 63, pp. 75–83.
15. M. Rahimian, S. Milenkovic, and I. Sabirov: *Philos. Mag. Lett.*, 2014, vol. 94, pp. 86–94.
16. Y. Zhang, B. Huang, and J. Li: *Metall. Mater. Trans. A*, 2013, vol. 44A, pp. 1641–44.
17. W. Kurz and D.J. Fisher: *Fundamentals of Solidification*, 4th ed., Trans Tech Publications, Aedermannsdorf, Switzerland, 1998.
18. A. Szcotok and K. Rodak: *IOP Conf. Ser. Mater. Sci. Eng.*, 2012, vol. 35, p. 012006.
19. L. Liu, F. Sommer, and H.Z. Fu: *Scripta Metall. Mater.*, 1994, vol. 30, pp. 587–91.
20. L.Z. He, Q. Zheng, X.F. Sun, G.C. Hou, H.R. Guan, and Z.Q. Hu: *J. Mater. Sci.*, 2005, vol. 40, pp. 2959–64.
21. S.M. Seo, J.H. Lee, Y.S. Yoo, C.Y. Jo, H. Miyahara, and K. Ogi: *Metall. Mater. Trans. A*, 2011, vol. 42A, pp. 3150–59.
22. C. Liu, J. Shen, J. Zhang, and L. Lou: *J. Mater. Sci. Technol.*, 2010, vol. 26, pp. 306–10.
23. S. Milenkovic, I. Sabirov, and J. Llorca: *Mater. Lett.*, 2012, vol. 73, pp. 216–19.
24. S. Milenkovic, M. Rahimian, and I. Sabirov: *Metall. Mater. Trans. B*, 2014, vol. 45B, pp. 482–88.
25. K.L. Gasko, G.M. Janowski, and B.J. Pletka: *Mater. Sci. Eng. A*, 1988, vol. 104, pp. 1–8.